



# Effect of nickel aluminide on the bainite transformation in a Fe-0.45C–13Ni–3Al–4Co steel, and associated properties

G.M.A.M. El-Fallah\*, S.W. Ooi, H.K.D.H. Bhadeshia

Materials Science and Metallurgy, University of Cambridge, 27 Charles Babbage Road, Cambridge, CB3 0FS, UK



## ARTICLE INFO

### Keywords:

nanostructured bainite  
Nucleation kinetics  
Intermetallic compounds  
Dilatometry  
toughness  
Strength

## ABSTRACT

It is known that precipitates that are present in austenite can influence its subsequent transformation behaviour. This investigation deals specifically with the role of nickel aluminide precipitates on the rate of the bainite reaction, in recent alloys intended for applications at about 400°C. It is demonstrated that the aluminides lead to an increase in the nucleation kinetics of the bainite. Furthermore, their presence increases the total quantity of bainite that forms, thus helping to reduce the scale of the austenite retained in the final microstructure. There is therefore, an increase in the fracture and impact toughnesses without sacrificing the strength. Diffraction experiments show that the retained austenite is optimally stable during the tensile test of the alloy containing NiAl.

## 1. Introduction

The driving force for the bainite transformation is affected by the solute content of the parent austenite. Elements in solid solution, such as manganese, chromium, molybdenum and vanadium [1,2] reduce the difference in free energy between the austenite and ferrite, and hence delay its transformation. The effect of elements that are in solid solution is essentially on the relative thermodynamic stabilities of the austenite and ferrite. However, precipitates in a variety of scenarios, can alter the kinetics by providing heterogeneous nucleation sites or by depleting the matrix [1,3–10].

In steels where there is a substantial concentration of nickel and aluminium, it is possible during heat treatments at temperatures above 500 °C to precipitate NiAl in the austenite [11–13]. Past investigations have dealt primarily with its precipitation in martensite or ferrite, as methods for enhancing strength [12–16]. We recently have developed such a steel for elevated temperature service, in which bainite is generated at a sufficiently high temperature where NiAl may also precipitate [13,17]. Stability at high temperatures is achieved by alloying with a large concentration of nickel which has the well-known austenite stabilising effect, and indeed, allows reversion to austenite if the temperature is sufficiently high [17]. The aluminium addition not only is essential for NiAl precipitation, but also greatly retards the precipitation of cementite [18–21], which would in turn cause the austenite to decompose. The iron-based alloy has the nominal chemical composition Fe-0.45C–13Ni–3Al–4Co wt%; the detailed composition is presented later. The purpose of this work is to study the effect of the NiAl

precipitation in austenite on the bainite transformation itself. The transformed steel is then subjected to mechanical tests to establish a structure-property relationships.

## 2. Material and experimental procedure

The composition of the alloy investigated is shown in Table 1. It was designed to exploit a mixed structure of fine bainitic ferrite embedded in carbon-enriched retained austenite, for a potential jet-engine shaft application. This necessitated a detailed study of its thermal stability [22] and mechanical behaviour at ambient and elevated temperatures [17]. The steel has enough carbon and nickel to guarantee a low transformation temperature which is conducive to the production of nanostructured bainite [23]. It also is rich in cobalt and aluminium, both of which accelerate the bainite transformation [24]. Molybdenum is added in a small concentration to prevent any possibility of phosphorus-induced embrittlement of the austenite grain boundaries [25].

The presence of both nickel and aluminium enable the formation of NiAl intermetallic compound in this alloy. An equilibrium thermodynamic calculation shows that NiAl can form in austenite between 550 °C, and 800 °C, Fig. 1a. The aim here was to investigate the effect of NiAl precipitation in austenite, on its subsequent transformation into bainite. In order to induce NiAl formation, the austenite was cooled and held at 740 °C. Fig. 1b shows the composition of the  $\beta$  – NiAl as a function of temperature.

The steel was produced by casting and hot-rolling into plate 120 mm × 20 mm × 600 mm. Dilatometric samples with a diameter of

\* Corresponding author.

E-mail address: [gmae2@cam.ac.uk](mailto:gmae2@cam.ac.uk) (G.M.A.M. El-Fallah).

**Table 1**  
Chemical composition of the steel investigated, wt%.

C	Si	Ni	Al	Mo	Mn	Co	P	N	Fe
0.45	0.030	13.20	2.63	0.30	0.15	3.99	0.006	0.0023	balance

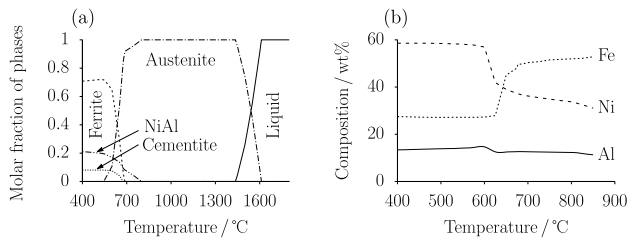


**Fig. 1.** Thermodynamic modelling using the software *MatCalc* with the Fe database version 5.62 to predict (a) stable phase fractions with liquid, austenite, ferrite, cementite and NiAl allowed to exist in the calculations. (b) Composition of the  $\beta$  – NiAl as a function of temperature.

4 mm and a length 10 mm, were machined from the mid-radius position of the hot rolled plate. The dilatometric investigation was performed in a Bähr DIL 805 A dilatometer. Temperature, diameter and change in length were monitored.

Four separate heat treatments were carried out as illustrated schematically in Fig. 2. Heat Treatment – I involved heating the samples at 5 °C s<sup>-1</sup> to 740 °C, 800 °C, and 850 °C, where they were held for 1 h, followed by cooling to room temperature at the same rate. The purpose was to determine whether the alloy is fully transformed into austenite at the holding temperature. The presence of cementite would reduce the amount of carbon available for the subsequent transformation. The martensite – start temperature ( $M_s$ ) was measured beginning with the fully austenitic state cooled at 5 °C s<sup>-1</sup>.

Another heat treatment (Fig. 2b) promotes NiAl at 740 °C, consistent with the calculations in Fig. 1a. The treatment illustrated in Fig. 2c additionally involves isothermal bainite formation prior to cooling to ambient temperature; Fig. 2d is similar to Fig. 2c but without the intermediate treatment that precipitates NiAl before the transformation to bainite. The heat treatments implemented on the dilatometer were replicated using a box furnace and fluidised bed on bigger samples for mechanical characterisation.

Transformation temperatures were determined by slope changes in the dilatometric curve, using the offset method [26]. For comparison with the measured bainite kinetic and martensite-start temperatures, time-transformation-temperature (TTT) as well as both bainite and martensite-start temperatures were calculated using in-house developed algorithms [27,28].

Samples mounted in conductive bakelite were ground using silicon carbide emery papers (600-grade to 2500-grade), followed by polishing with 6 to 1 μm diamond paste, the polishing is finished with 0.25 μm colloidal silica. Scanning electron microscopy of FEI Nova NanoSEM operating at 15 kV and Olympus optical microscope are used for microstructure investigation. Etching was performed with a 2% nitric acid, 98% methanol mixture.

Unmounted sections were similarly prepared for X-ray analysis but without etching. X-ray diffraction analysis (Cu K $\alpha$  radiation) was used to determine the fraction of retained austenite and bainitic ferrite. The step size was 0.050 ° with a dwell time of 5 s, 2.5 ° primary slit, a divergence slit 8 mm wide and 18 mm antiscatter slit at 40 kV and 40 mA and a rotational speed was 30° min<sup>-1</sup>. The obtained X-ray spectrum were subjected to Rietveld refinement [29]. The weighted profile  $R$ -factor ( $R_{wp}$ ) and goodness-of-fit were used to assess the quality of the

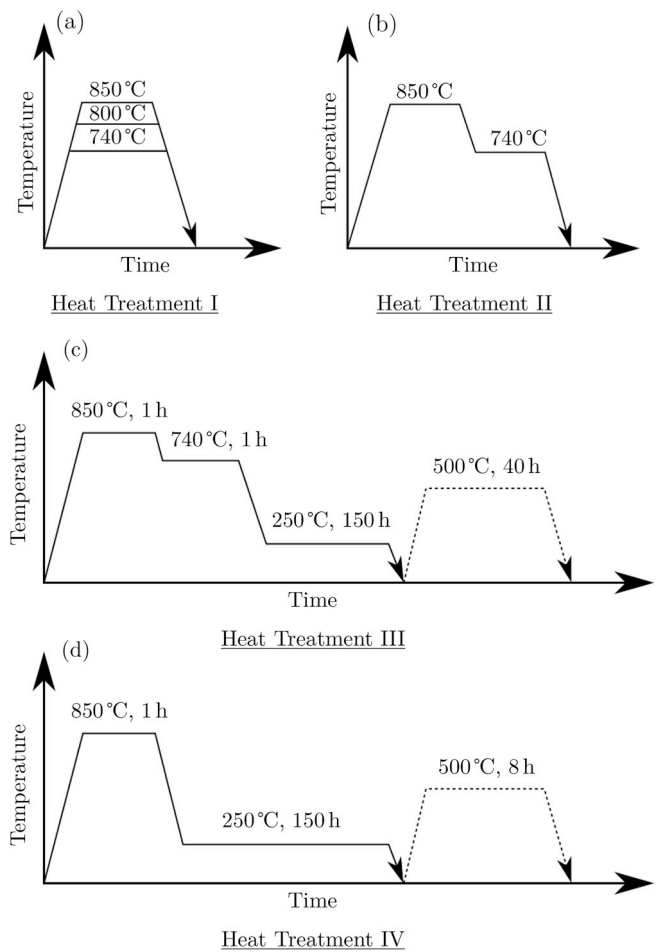


**Fig. 2.** Heat treatments carried out using a dilatometer, box furnace and a fluidised bed. Arrows indicate the quench to room temperature using a jet of argon gas or free-air cooling. (a, b) The purpose here was to measure the ( $M_s$ ) temperature after austenitisation and to ensure all cementite is dissolved. (c, d) To investigate and compare the effect of NiAl on bainite transformation and on the mechanical properties of this alloy in the as-transformed bainitic and tempered conditions.

fitting, which also checked graphically [30]. The Dyson and Holmes [31] relationship between the austenite composition and its lattice parameter was used to estimate its carbon content. Vicker's hardness determinations used a 10 kg load, taking the average of six indents in each case.

Samples for the orientation imaging were ground and electro-polished at 11 V for 8 min. Crystallographic data were produced by electron backscatter diffraction (EBSD) using a ZEISS GeminiSEM 300 field emission gun scanning electron microscope at a magnification of  $\times$  1500 with a step size of 0.06 μm. Data analysis was carried out using “Channel 5” software. A FEI Tecnai Osiris operated at 200 keV was used for transmission microscopy. Electropolishing of thin foils was performed using 5% perchloric acid, 25% glycerol and 70% ethanol at 8.5 °C and 25 V.

Toughness was measured using crack-tip opening displacement (CTOD) fracture toughness (Fig. 3a) and standard 10 mm  $\times$  10 mm Charpy impact tests. Both tests were performed in accordance with ASTM E399-09 and ASTM E23-12c respectively. Tensile tests were carried out at ambient temperature (Fig. 3b), and testing method described in Ref. [17].

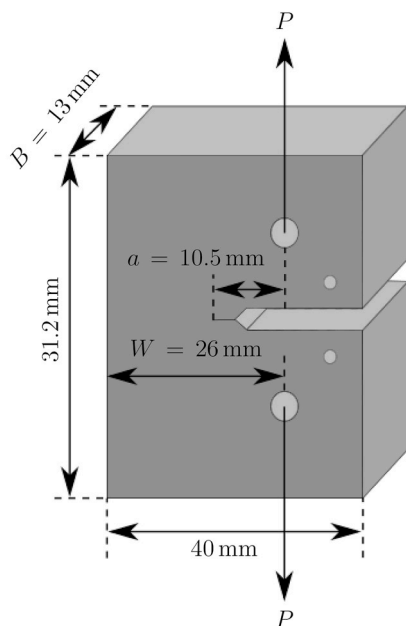


**Fig. 3.** Sample geometries for (a) fracture toughness (compact tension) testing. Where  $P$  is the load and  $a$ ,  $B$  and  $W$  refer to the measurements used in Ref. [32]. (b) Tensile testing. All testpieces were machined from the centre of each blank after heat treatment.

### 3. Results

#### 3.1. Dilatometry

The dilatometric curve of the as-received martensitic material, Fig. 4a, shows two contractions during heating to 850 °C, at  $\approx 500$  °C and  $\approx 700$  °C. The first is as the martensite tempers to precipitate cementite. To test this, a sample that was heated to just 600 °C at  $5$  °C,  $s^{-1}$  before cooling to ambient temperature, followed by reheating up to 850 °C, which eliminated the contraction as shown in Fig. 4b. Metallographic observations confirm the temperature at which the cementite forms, Fig. 4c.

The second contraction is due to austenite growth, Fig. 4d. The data indicate that the alloy is essentially austenitic at 730 °C, Fig. 4d. However, the microstructural evidence suggests otherwise. Fig. 5 shows that cementite that forms during reheating is not completely dissolved after holding for 1 h at 740 °C and 800 °C. And indeed, the dilatometry data Fig. 6 confirm in a preliminary manner, that the transformation

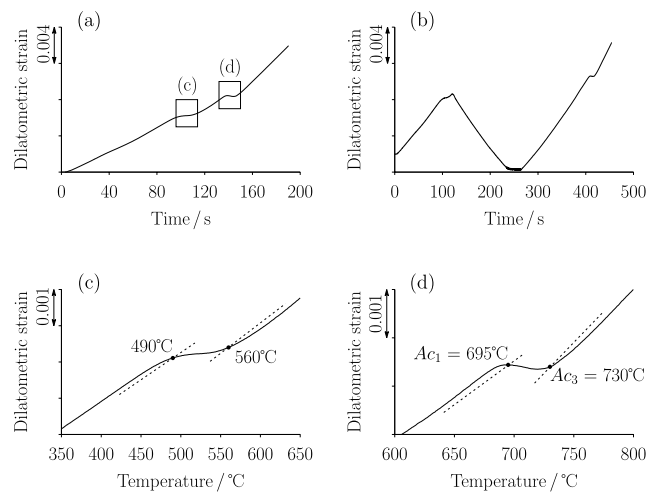


**Fig. 4.** Dilatometry curves during heating an initially martensitic microstructure. (a) The fraction of cementite and austenite formation during heating at  $5$  °C  $s^{-1}$  to 850 °C. (b) The cementite contraction disappears during heating the sample at 600 °C then reheating to 850 °C without holding. (c) Beginning and the end of cementite formation during heating and (d) austenite start and finish temperatures  $A_{c1}$  and  $A_{c3}$  respectively during heating.

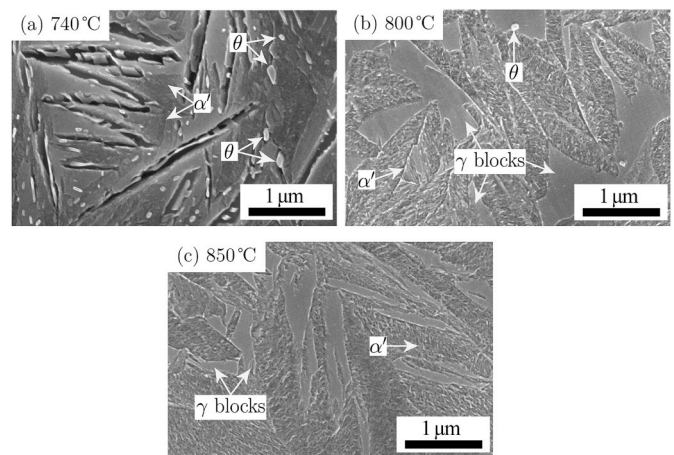


**Fig. 5.** Microstructures after austenitisation at temperature indicated according to Heat Treatment I Fig. 2a.  $\alpha'$ ,  $\theta$  and  $\gamma$  represent martensite, cementite and austenite respectively. (a) The structure consists of large martensite plates. (b) Martensite plate and intervening regions of austenite. Cementite not fully dissolved at 740 °C and 800 °C. (c) Martensite plates and austenite grain boundaries. No sign of cementite, which has dissolved when the steel is heated up at 850 °C.

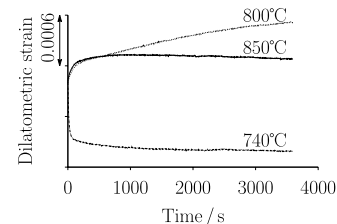


**Fig. 6.** Austenite transformation experiments during holding for 1 h at different temperatures as indicated. This alloy is predicted to be completely austenitic at 850°C; at 800°C the cementite not fully dissolved, and 740°C indicates that the austenite transformation does not reach completion.

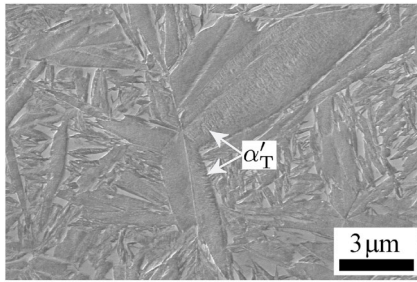


**Fig. 7.** Microstructures after austenitisation according to Heat Treatment II Fig. 2b. Large martensite plates exhibiting twins  $\alpha'_T$ . No cementite formation after holding at 740°C.

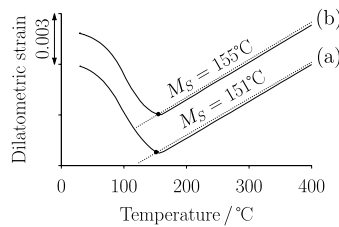


**Fig. 8.** Cooling dilatometric curve showing the martensite starting temperature  $M_s$ . (a) One step austenitisation at 850 °C of a period of 1 h. (b) Two step austenitisation at 850 °C for 1 h then 740 °C for 1 h where NiAl formation is promoted. Both samples were cooled to room temperature at 5°C s<sup>-1</sup>.

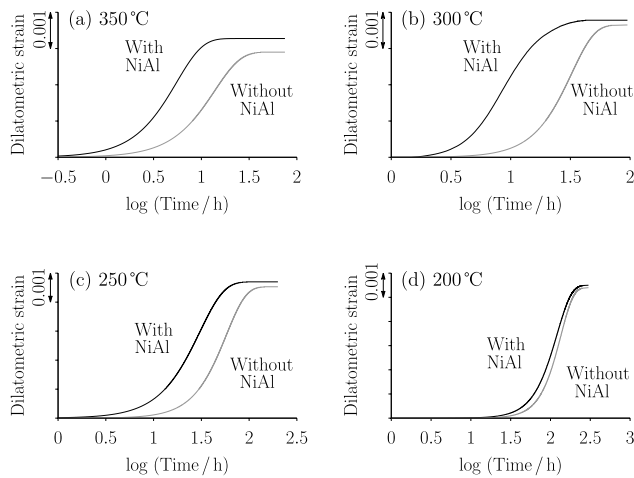


**Fig. 9.** Isothermal reaction curves showing that the presence of NiAl not only accelerates transformation but can lead to a greater ultimate quantity of bainite.

**Table 2**

The transformation-start time is shorter when the austenite contains NiAl precipitates. “ $\Delta t$ ” refers to the difference in transformation – start time between the samples contain NiAl and without NiAl.

Isothermal transformation temperature/°C	Transformation – start time/h		$\Delta t$ /h
	With NiAl	Without NiAl	
350	0.9	2.7	1.8
300	2.8	6.3	3.5
250	4	11.5	7.5
200	29	35	6

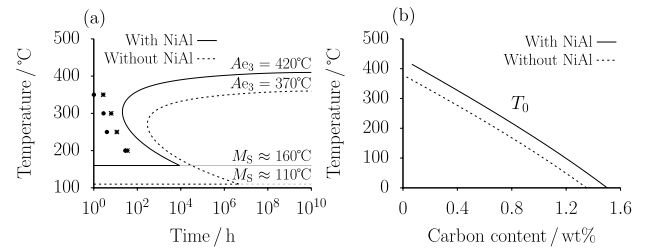


**Fig. 10.** (a) TTT curve calculated using MTTData [33]. Points [•] and [\*] are the bainite transformation start time obtained experimentally with and without NiAl precipitates respectively. (b)  $T_0$  calculated using MTTData, larger volume fraction of bainitic ferrite due to the precipitation of NiAl.

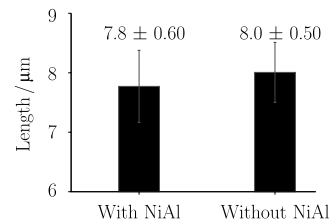


**Fig. 11.** The average apparent-length of 100 bainite sheaves. The samples were transformed isothermally at 250 °C for 10 h followed by quenching to ambient temperature.

does not reach completion during holding at 740 °C and cementite cannot be fully dissolved at 800 °C. Accordingly, the austenitisation temperature of 850 °C is chosen for subsequent investigations so that austenitisation can be completed before NiAl precipitation. Fig. 7 shows that the microstructure after the two austenitisation stages does not contain any cementite particles. Fig. 8 shows that  $M_s$  is 151 °C, for one step austenitisation, and 155 °C, for the two-step austenitisation where NiAl formation is stimulated.

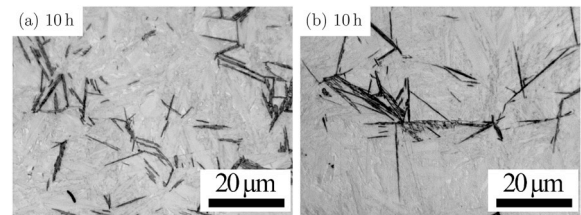


**Fig. 12.** Micrographs of partial bainitic transformation at 250 °C and interrupting at the time indicated (a) with NiAl. (b) Without NiAl.

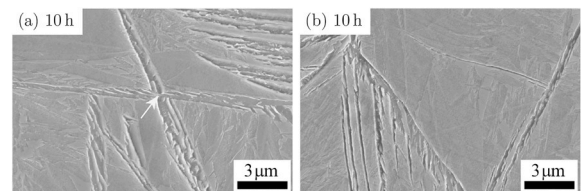


**Fig. 13.** SEM of partial bainitic transformation, formed after transformation at 250 °C and interrupting at the time indicated (a) with NiAl arrow indicates the intragranular nucleation of bainite from the NiAl precipitates. (b) Without NiAl, nucleation is from the austenite grain boundaries.

### 3.2. Kinetics of the bainite transformation

The effect of NiAl on the bainite transformation kinetics is shown in Fig. 9 and some transformation-start times are listed in Table 2. The reaction is clearly more rapid in the presence of NiAl precipitates; for example, the difference in the transformation start time ( $\Delta t$ ) is 7.5 h during transformation at 250 °C, Fig. 9c. Furthermore, the net amount of bainite obtained is greater when the NiAl is present prior to the bainite transformation.

A thermodynamic model MTTTDATA (which is a combination of mugg83 and MTDATA thermodynamics database software) has been developed to allow the estimation of isothermal transformation in high alloy steels [33]. Thermodynamic data are retrieved from a database to facilitate kinetic predictions [34]. Fig. 10, shows that the transformation-start times obtained experimentally are somewhat shorter than

those calculated. Transformation curves on TTT diagrams Fig. 10a are consistent with the hypothesis that the difference in the reaction rate peaks at intermediate isothermal transformation temperature. The diffusion of atoms becomes difficult at low temperatures whereas the driving force for transformation is reduced as the temperature is raised. Therefore, the reaction rates are slow both at high temperatures (300 and 350 °C) and low temperature (200 °C). Fig. 10a shows that the calculated  $B_s$  and  $M_s$  are higher when the steel contains NiAl before transformation. The chemical composition of the matrix used to investigate the effect of NiAl of the austenite on transformation temperature is obtained from the Matcalc calculation at 740 °C.

A locus of the  $T_0$  temperature as a function of the carbon concentration is plotted in Fig. 10b. This also indicates that a higher amount of bainite transformation is expected in the presence of NiAl, Fig. 9. This is because the  $T_0$  curve is shifted to a higher carbon

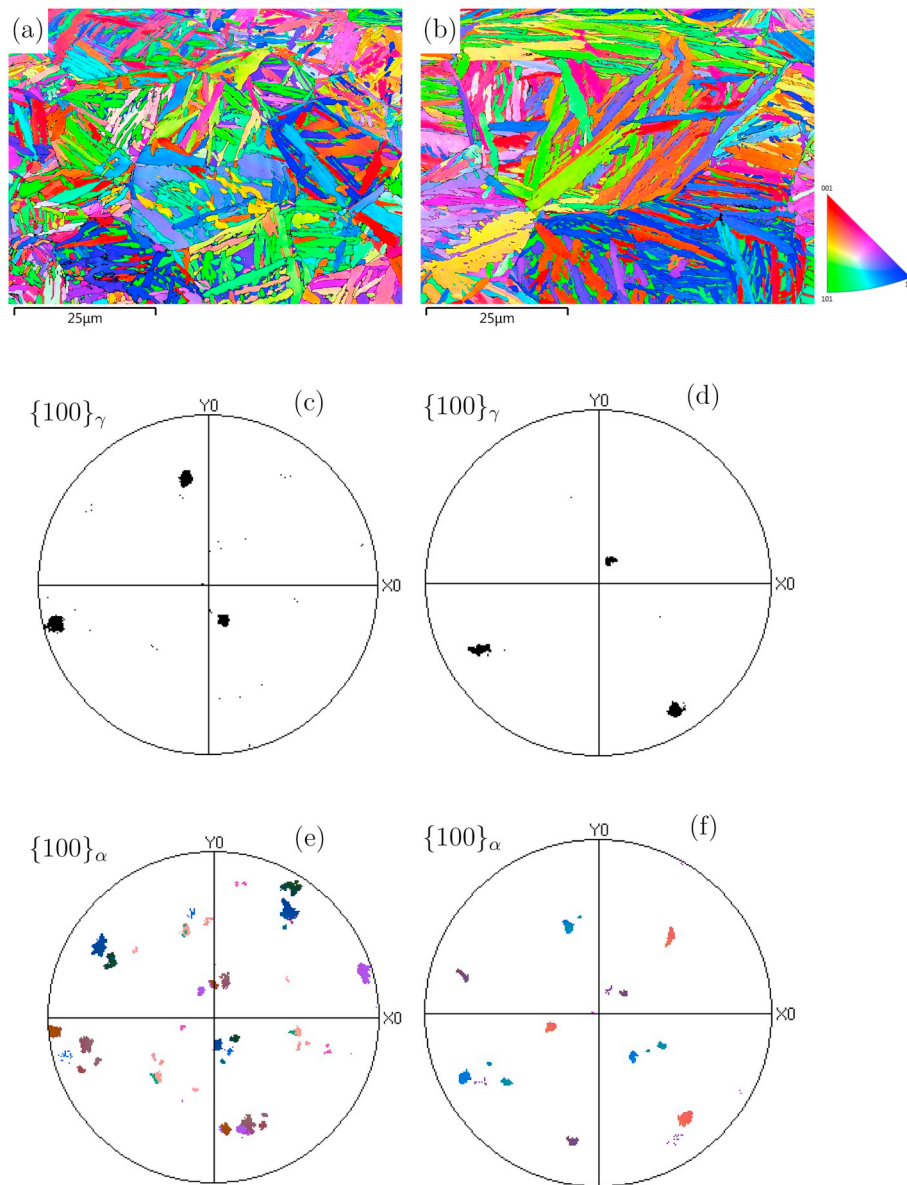


Fig. 14. EBSD orientation image, sample transformed isothermally at 250 °C for 150 h followed by cooling to ambient temperature. (a) Bainite nucleated from NiAl promotes a more chaotic and finer bainite structure. (b) Grain boundary nucleated bainite. Pole figures from a parent austenite grain, (c, d)  $\{100\}_\gamma$  pole figure, (e, f) corresponding  $\{100\}_\alpha$  pole figure, more variants within the austenite grain (e).

concentration by altering the chemical composition of the austenite. The presence of NiAl clearly increases the amount of bainite transformation, which helps reduce the blocks of austenite.

To test whether the primary role of NiAl precipitates is to stimulate nucleation, the apparent lengths of bainite sheaves were measured following partial transformation at 250 °C. Fig. 11 shows that there is no significant difference with and without the NiAl, confirming that the particles promote transformation by providing heterogeneous nucleation sites.

Fig. 12 shows microstructural evidence of the greater degree of transformation achieved in the given time, when NiAl precipitates in austenite. Fig. 13a shows evidence for the intergranular nucleation of  $\alpha_b$  on NiAl, leading to significantly different microstructure compared with austenite grain boundary dominated nucleation (Fig. 13b). This also can be observed from the EBSD orientation images in Fig. 14, where the NiAl promotes a more chaotic and finer bainite structure compared to the NiAl-free sample. The corresponding pole figures show the spread in bainite orientation within an individual austenite grain is greater on the sample with prior NiAl precipitation. Higher magnification images are provided as supplemental data (A and B).

The structure consists of austenite and bainite plates with fine precipitates ( $\approx 100$  nm) of NiAl embedded in the bainite plates (Fig. 15). The  $\beta$  - NiAl is confirmed by electron diffraction, Fig. 15c, where superlattice reflections are observed due to primitive cubic crystal structure with a motif of Ni at 0, 0, 0 and Al at  $\frac{1}{2}$ ,  $\frac{1}{2}$ ,  $\frac{1}{2}$  associated with each lattice point. Energy dispersive spectroscopy

confirmed that the fine precipitates are rich in nickel and aluminium Fig. 15d.

Vickers hardness tests as a function of fraction of bainite performed on dilatometric heat-treated samples are shown in Fig. 16, together with the measured phase fractions. The hardness ( $660 \pm 6$ HV) of the as-quenched microstructure is greater when NiAl precipitates are present compared with the sample without precipitates ( $594 \pm 4$ HV), with the amount of martensite being identical in both cases. Indicating that the increase in hardness is due to the formation of NiAl.

With interrupted bainite transformation, there are trends with regards to the hardness obtained. Fig. 16a shows that alloy without NiAl, the measured hardness slightly peaks as the fraction of martensite decreases. As the amount of bainite increases, so does the carbon concentration of the austenite; therefore, the hardness of any martensite that forms subsequently also increases resulting in the peak. However, when enough bainite formed (Fig. 16b) this effect diminishes because the austenite tends to be retained. Similar effects have been observed previously [35].

### 3.3. Toughness

All measured fracture toughness values are given in Table 3. The sample containing NiAl precipitates exhibits a toughness significantly higher  $\approx 15\%$  than the one without prior the precipitates, and it is so tough that valid measurements of  $K_{IC}$  were not possible. This also can be seen from (supplementary Fig. 21a), where the as-transformed

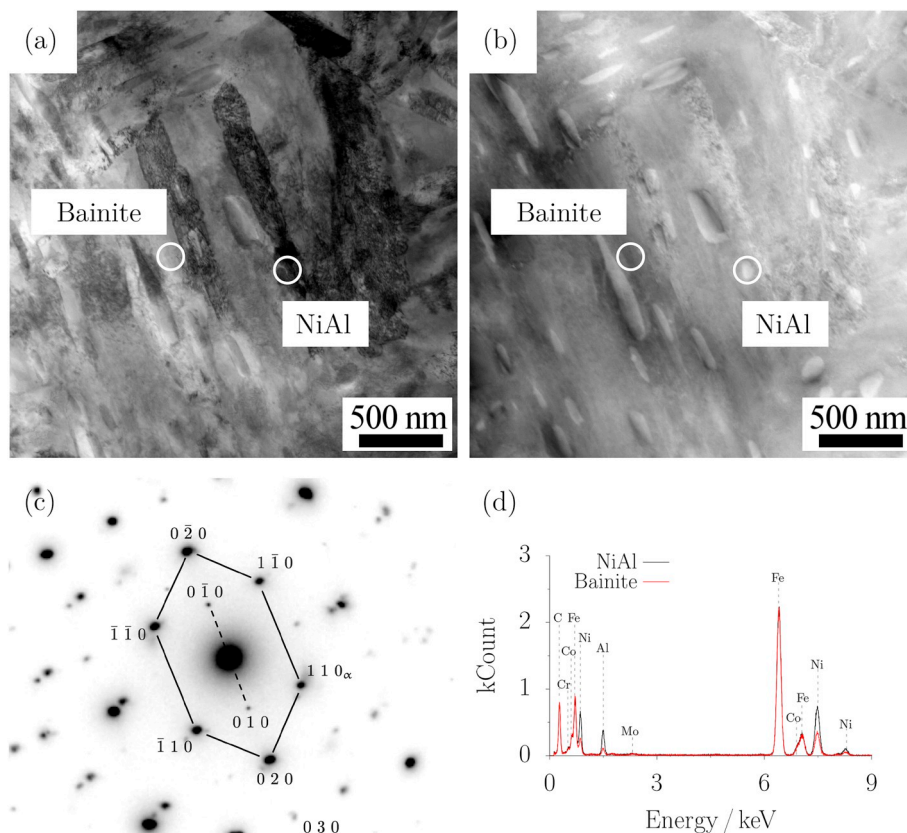
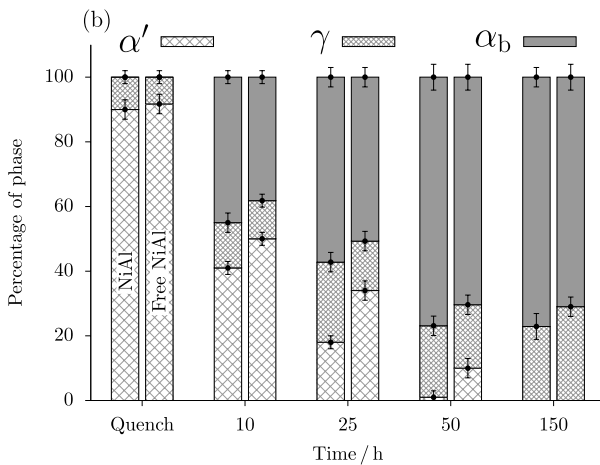
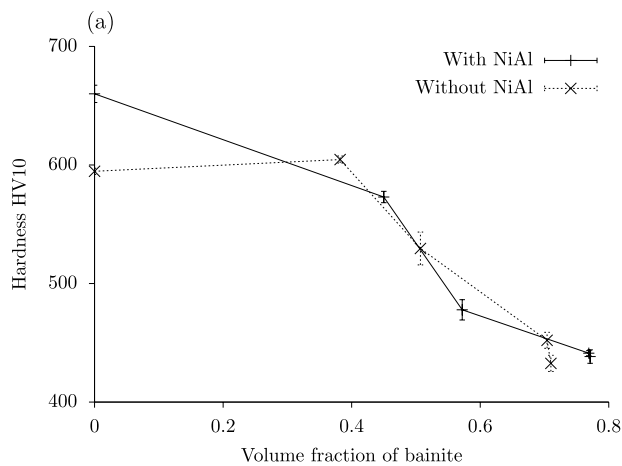


Fig. 15. STEM bright field image transformed isothermally at 250 °C for 150 h followed by cooling to ambient temperature. (a) Microstructure of austenite and bainitic ferrite plates with fine precipitates of NiAl embedded in the latter. (b) Corresponding dark HAADF STEM image elliptical  $\gamma'$  inclusion can be seen (light). Highlighted area used for EDS point scanning. (c) Corresponding superimposed electron diffraction pattern from [001] $_{\alpha}$  matrix and  $\gamma'$ . The  $\alpha$  matrix and  $\gamma'$  are, as expected, in cube - cube orientation. (d) EDS from the marked region showing enriched regions of aluminium and nickel in areas containing precipitates.



**Fig. 16.** (a) Vickers hardness as a function of volume fraction of bainite transformed isothermally at 250 °C. (b) Phase fractions determined using cooling dilatometric curves along with the X-ray data. 'Quench' samples represent the hardness of a mixture of martensite and austenite obtained by quenching from a fully austenitic state. Isothermal interrupted tests at 10, 25 and 50 h to fully bainitic microstructures at 150 h.  $\alpha'$ ,  $\gamma$  and  $\alpha_b$  represent martensite, austenite and bainite respectively.

**Table 3**

Fracture toughness and Charpy impact results measured in bainitic and tempered samples at ambient temperature according to heat treatment shown in Fig. 2.

Alloy with NiAl	Temper	$K_Q / \text{MPa m}^{\frac{1}{2}}$	$K_{Ic} / \text{MPa m}^{\frac{1}{2}}$	Impact energy/J
✓	×	70.9		32.5
	✓	18		2.7
×	×		60.1	22.4
	✓	18.2		2.7

sample containing NiAl precipitates exposed higher load and greater crack opening displacement compared with NiAl free sample (supplementary Fig. 21c). Charpy tests in (Table 3) confirmed these trends.

The fracture toughness values of the tempered bainite (with and without NiAl) are identical. This is because the exposure time has been chosen where both samples achieved the highest hardness value of  $\approx 607$  HV (Fig. 2c and d). This can be seen from (supplementary Fig. 21b and 21d), where both samples experienced equivalent applied

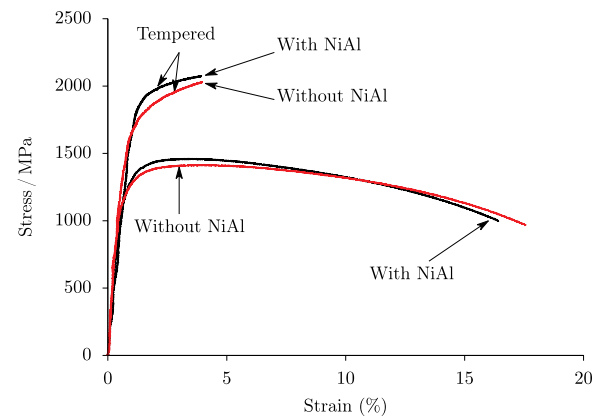


**Fig. 17.** Engineering stress-strain curves measured during tensile tests for as-transformed and tempered conditions at ambient temperature.

load. The fracture toughness values for the tempered samples containing NiAl and NiAl free are  $\approx 18 \text{ MPa m}^{\frac{1}{2}}$ , close to that of conventional nanostructured steels in the as-transformed condition [36–38]. Fractographs of fracture toughness and Charpy impact tests images are presented as supplemental data (D).

### 3.4. Tensile properties

Room-temperature tensile tests were performed in the as-transformed bainitic and tempered conditions. The resulting engineering stress-strain curves are presented in Fig. 17, with derived parameters summarised in Table 4. The samples containing NiAl precipitates are slightly stronger than those without NiAl precipitation in the as-transformed bainitic condition. It is evident that both microstructures can accommodate a significant plastic deformation before failure. A hardness comparison (Fig. 18) of the grip, gauge and fracture regions, shows that alloy contains NiAl samples tested at room temperature hardened slightly when compared with alloy without prior precipitation of the intermetallic particles.

The retained austenite is optimally stable during the tensile test consistent with the observed increase in the carbon concentration (Table 5) in the alloy contain NiAl. This also can be observed clearly from (Fig. 10b) where  $T_0$  curve is shifted to a higher carbon concentration. Furthermore, the steel without prior NiAl precipitates shows a decrease in the carbon concentration of the retained austenite in the unstressed gauge section, making the austenite less stable to martensitic transformation.

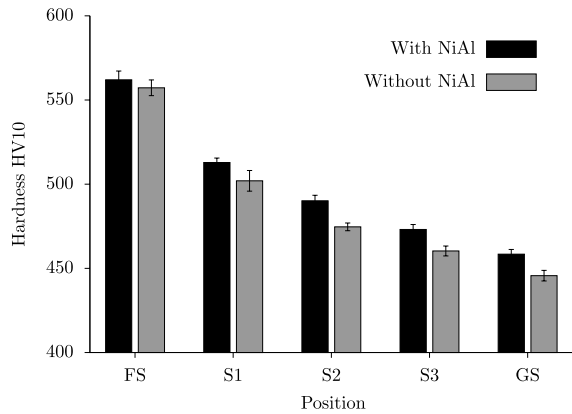
Tempering at 500 °C, also increases the 0.2% proof stress and ultimate tensile strength of both cases, consistent with the transformation of austenite to the less-ductile ferrite and the precipitation of cementite. Fractographs of tensile test images are presented as supplemental data (D).

## 4. Summary

All of the experimental results indicate that the formation of NiAl in the austenite accelerated the subsequent bainitic transformation. Since the sheaf length does not change significantly in the presence or absence of NiAl, it can be concluded that NiAl promotes the heterogeneous nucleation of bainite. This is because the acceleration of the bainite reaction in the presence of NiAl change the chemical composition of the austenite matrix. This also results in an increase in the amount of bainite which has the consequence of reducing the coarse regions of retained austenite. All of these factors lead to greater strength and toughness in the NiAl containing samples.

**Table 4**Tensile test results for as-transformed and tempered conditions tested at ambient temperature. All tests performed at a constant crosshead speed of 0.002 mm min<sup>-1</sup>.

Alloy with NiAl	Temper	E/ GPa	0.2% proof stress/MPa	$\sigma_{UTS}$ /MPa	Uniform elong. (%)	Failure elong. (%)	Red./of area (%)
✓	×	182	1245	1487	4.0	16.4	59.8
	✓	187	1767	2073	4.0	4.0	4.2
×	×	181	1123	1412	4.0	17.6	61.7
	✓	178	1508	2029	4.0	4.0	3.7

**Fig. 18.** Measured Vickers hardness of tensile test samples, using a 10 kg load. NiAl precipitates cause the alloy to hardened slightly compared with the free NiAl alloy.**Table 5**Diffraction data for both set of alloys tested at the ambient temperature. FS represents the fracture surface and GS is the undeformed area, (S1–S3) gauge sections.  $V_\gamma$  and  $C_\gamma$  stands for volume fraction and carbon content of austenite respectively and  $a_\gamma$  is the austenite lattice parameter.

Alloy with NiAl	Section	$V_\gamma$	$a_\gamma / \text{\AA}$	$C_\gamma / \text{wt}\%$
✓	FS	0.11 ± 0.02	3.6404 ± 0.0041	1.49 ± 0.02
	S1	0.18 ± 0.01	3.6354 ± 0.0031	1.34 ± 0.02
	S2	0.24 ± 0.02	3.6302 ± 0.0031	1.18 ± 0.01
	S3	0.25 ± 0.01	3.6292 ± 0.0029	1.15 ± 0.01
	GS	0.26 ± 0.02	3.6285 ± 0.0022	1.13 ± 0.01
×	FS	0.16 ± 0.02	3.6349 ± 0.0035	1.33 ± 0.02
	S1	0.20 ± 0.01	3.6321 ± 0.0030	1.24 ± 0.02
	S2	0.26 ± 0.01	3.6255 ± 0.0028	1.04 ± 0.01
	S3	0.27 ± 0.01	3.6241 ± 0.0023	1.00 ± 0.01
	GS	0.28 ± 0.01	3.6235 ± 0.0021	0.98 ± 0.01

## Acknowledgements

The authors would like to thank the Libyan Higher Education and Scientific Research for funding the work and Dr Mohammed Hassan Abu-Bakr for the support.

## Appendix A. Supplementary data

Supplementary data to this article can be found online at <https://doi.org/10.1016/j.msea.2019.138362>.

## References

- [1] C. Zener, Kinetics of the decomposition of austenite, *Trans. Am. Inst. Min. Metall. Eng.* 167 (1946) 550–595.
- [2] Secretary of State for Defence, H.K.D.H. Bhadeshia, C. Mateo, P. Brown, *Bainite Steel and Methods of Manufacture Thereof*, Technical Report {GB}2462197, Intellectual Property Office, London, U.K., 2010.
- [3] S. Jin, J.W. Morris, Y.L. Chen, G. Thomas, R.I. Jaffee, An investigation of

transformation strengthening in precipitation-hardened Fe-Ni austenite, *Metall. Trans. A* 9 (1978) 1625–1633.

- [4] J.M. Dowling, J.M. Corbett, H.W. Kerr, Inclusion phases + nucleation of acicular ferrite in SMA welds, *Metall. Trans. A* 17 (1986) 1611–1623.
- [5] A. Ali, H.K.D.H. Bhadeshia, Aspects of the nucleation of {W}idmanstätten ferrite, *Mater. Sci. Technol.* 6 (1990) 781–784.
- [6] G.I. Rees, J. Perdrix, T. Maurickx, H.K.D.H. Bhadeshia, The effect of niobium in solid solution on the transformation kinetics of bainite, *Mater. Sci. Eng. A* 194 (1995) 179–186.
- [7] H. Mabuchi, R. Uemori, M. Fujioka, Role of Mn depletion in intra-granular ferrite transformation in the heat affected zone of welded joints with large heat input in structural steels, *ISIJ Int.* 36 (1996) 1406–1412.
- [8] J.M. Gregg, H.K.D.H. Bhadeshia, Solid-state nucleation of acicular ferrite on minerals added to molten steel, *Acta Mater.* 45 (1997) 739–748.
- [9] T. Furuhashi, J. Yamaguchi, N. Sugita, G. Miyamoto, T. Maki, Nucleation of proeutectoid ferrite on complex precipitates in austenite, *ISIJ Int.* 43 (2003) 1630–1639.
- [10] H. Hu, G. Xu, L. Wang, Z. Xue, Y. Zhang, G. Liu, The effects of Nb and Mo addition on transformation and properties in low carbon bainitic steels, *Mater. Sci. Eng. A* 84 (2015) 95–99.
- [11] C. Stallybrass, A. Schneider, G. Sauthoff, The strengthening effect of (ni,fe)al precipitates on the mechanical properties at high temperatures of ferritic fe–al–ni–cr alloys, *Intermetallics* 13 (12) (2005) 1263–1268 (Discussion Meeting on the Development of Innovative Iron Aluminium Alloys).
- [12] Z.B. Jiao, J.H. Luan, M.K. Miller, C.T. Liu, Precipitation mechanism and mechanical properties of an ultra-high strength steel hardened by nanoscale nial and cu particles, *Acta Mater.* 97 (2015) 58–67.
- [13] C.N. Hulme-Smith, S.W. Ooi, H.K.D.H. Bhadeshia, Intermetallic-strengthened nanocrystalline bainitic steel, *Mater. Sci. Technol.* 34 (16) (2018) 1976–1979.
- [14] R. Prakash Kolli, David N. Seidman, The temporal evolution of the decomposition of a concentrated multicomponent fe–cu-based steel, *Acta Mater.* 56 (9) (2008) 2073–2088.
- [15] M. Kapoor, D. Isheim, S. Vaynman, M.E. Fine, Y.-W. Chung, Effects of increased alloying element content on nial-type precipitate formation, loading rate sensitivity, and ductility of cu- and nial-precipitation-strengthened ferritic steels, *Acta Mater.* 104 (2016) 166–171.
- [16] Z.B. Jiao, J.H. Luan, W. Guo, J.D. Poplawsky, C.T. Liu, Atom-probe study of cu and nial nanoscale precipitation and interfacial segregation in a nanoparticle-strengthened steel, *Mater. Res. Lett.* 5 (8) (2017) 562–568.
- [17] G.M.A.M. El Fallah, H.K.D.H. Bhadeshia, Tensile behaviour of thermally-stable nanocrystalline bainitic-steels, *Mater. Sci. Eng. A* 746 (2019) 145–153.
- [18] A.G. Allen, Discussion to “the effect of silicon on the kinetics of tempering”, *Trans. ASM* 46 (1954) 812–829.
- [19] E.W. Langer, An investigation of carbide precipitation in iron, *Met. Sci. J.* 2 (1968) 59–66.
- [20] M.S. Bhat, *Microstructure And Mechanical Properties of AISI 4340 Steel Modified with Al And Si*, PhD Thesis, Lawrence Berkley Laboratories, California, USA, 1977.
- [21] H.K.D.H. Bhadeshia, *Cementite*, *Int. Mater. Rev.* 64 (2019), <https://doi.org/10.1080/09506608.2018.1560984>.
- [22] C.N. Hulme-Smith, H.K.D.H. Bhadeshia, Mechanical properties of thermally-stable, nanocrystalline bainitic steels, *Mater. Sci. Eng. A* 700 (2017) 714–720.
- [23] F.G. Caballero, H.K.D.H. Bhadeshia, Very strong bainite, *Curr. Opin. Solid State Mater. Sci.* 8 (2004) 251–257.
- [24] H.I. Aaronson, H.A. Domian, Partitioning of alloying elements between austenite and proeutectoid ferrite and bainite, *TMS-AIME* 236 (1966) 781–796.
- [25] R.H. Greaves, J.A. Jones, Temper brittleness of steel; susceptibility to temper brittleness in relation to chemical composition, *J. Iron Steel Inst.* 111 (1925) 241–255.
- [26] H.-S. Yang, H.K.D.H. Bhadeshia, Uncertainties in the dilatometric determination of the martensite-start temperature, *Mater. Sci. Technol.* 23 (2007) 556–560.
- [27] H.K.D.H. Bhadeshia, S.A. David, J.M. Vitek, R.W. Reed, Stress induced transformation to bainite in Fe-Cr-Mo-C pressure vessel steel, *Mater. Sci. Technol.* 7 (1991) 686–698.
- [28] H.K.D.H. Bhadeshia, Thermodynamic extrapolation and the martensite-start temperature of substitutionally alloyed steels, *Met. Sci.* 15 (1981) 178–180.
- [29] H.M. Rietveld, A profile refinement method for nuclear and magnetic structures, *J. Appl. Crystallogr.* 2 (1969) 65–71.
- [30] B.H. Toby, R factors in Rietveld analysis: how good is good enough? *Powder Diffr.* 21 (01) (2006) 67–70.
- [31] D.J. Dyson, B. Holmes, Effect of alloying additions on the lattice parameter austenite, *J. Iron Steel Inst.* 208 (1970) 469–474.
- [32] G.E. Dieter, *Mechanical Metallurgy*, McGraw-Hill Book Company Limited, U. K,

- 1988.
- [33] T. Okumura, MAP\_STEEL\_MTTTDATA, <http://www.msm.cam.ac.uk/map/steel/programs/MTTTDATA.html>, (2004).
- [34] H.K.D.H. Bhadeshia, Thermodynamic analysis of isothermal transformation diagrams, *Met. Sci.* 16 (1982) 159–165.
- [35] Y. Tomita, K. Okabayshi, Improvement in lower temperature mechanical properties of 0.40 Pct C-Ni-Cr-Mo ultrahigh strength steel with 2nd phase, *Metall. Trans. A* 14 (1983) 485–492.
- [36] F.G. Caballero, C. Garcia-Mateo, Ultra-high – strength bainitic steels, *ISIJ Int.* 45 (11) (2005) 1736–1740.
- [37] C. Garcia-Mateo, F.G. Caballero, H.K.D.H. Bhadeshia, Mechanical properties of low-temperature bainite, *Mater. Sci. Forum* 500–501 (2005) 495–502.
- [38] F.G. Caballero, J. Chao, J. Cornide, C. Garcia-Mateo, M.J. Santofimia, C. Capdevila, Toughness deterioration in advanced high strength bainitic steels, *Mater. Sci. Eng. A* 525 (1–2) (nov 2009) 87–95.